Vibrational Analysis of Carbon Nanotube Based Nanomechanical Resonators

Nicholas A. Besley*

School of Chemistry, University of Nottingham, University Park, Nottingham, NG7 2RD, UK.

E-mail: nick.besley@nottingham.ac.uk

Abstract

A vibrational analysis of three types of carbon nanotube based nanomechanical resonator is presented. Harmonic vibrational frequencies and the associated normal modes are evaluated through diagonalisation of the full mass-weighted hessian matrix where a very large mass is assigned to the suitable carbon atoms to represent the constraints arising as a consequence of the different resonator configurations. The vibrational frequencies are determined for carbon nanotubes of different dimensions, and the response of the resonators to an applied mass is studied. For the flexural modes which are relevant for mass-sensing resonator devices, the calculations show the resonant frequency to increase as the tube diameter increases. For the longest nanotubes studied, the frequencies for cantilever and bridged resonators are very similar, and double-walled nanotubes have resonant frequencies that lie between the frequencies of the component single-walled nanotubes. The vibrational modes for a shuttle resonator have also been determined, and the lowest frequency mode was found to correspond to the relative rotation of the nanotubes with frequencies in the range 70 – 120 GHz. The calculations predict a sensitivity of up to 10^{30} Hz/g although the response of the flexural modes of suspended nanotubes is dependent on the location of the adsorbed

mass, while the response based upon the relative rotational motion in double-walled nanotubes is independent of the position of the adsorbed mass.

Introduction

There is considerable interest in nanomechanical resonators based upon carbon nanotubes (CNTs).[1–5] The high stiffness and strength coupled with low density of CNTs make them attractive candidates for these devices. One area of application of these resonators is in sensing devices which have the potential to greatly advance fundamental measurements at the molecular scale. One prominent example is the use of CNT-based resonators as highly sensitive mass detection devices.[1,6–12] These devices have resonant frequencies of the order of giga-hertz and function by measuring the change in frequency induced by the change in the effective mass of the resonator when a particle adsorbs. The exceptional sensitivity of these devices has the potential to achieve atomic resolution, for example in the detection of gold atoms.[7] There are several possible configurations for a nanomechanical resonator, and three types are illustrated in Figure 1. In a cantilever resonator, one end of the nanotube is clamped and fixed in position and the remainder of the nanotube is free to vibrate. In a bridged resonator both ends of the nanotube are clamped and the central part of the nanotube is free to vibrate. Figure 1 illustrates these resonators for single-walled nanotubes, however, these resonators can also be constructed based upon double-walled (or multi-walled) nanotubes. In these resonators, the ends of all of the nanotubes are fixed in position. The majority of work on these devices has focused on the flexural modes of cantilever or bridged type of resonator. In this study, a third type of device, denoted shuttle, proposed in earlier work[13,14] is considered. This resonator is based upon two nanotubes, where the inner nanotube is clamped and a second shorter nanotubes is free move around the inner nanotube, and the vibrational modes of interest involve the relative motion between the walls of the nanotubes. One advantage of this type of device is that the shift in frequency should be

insensitive to the location of the adsorbed particle on the resonator.

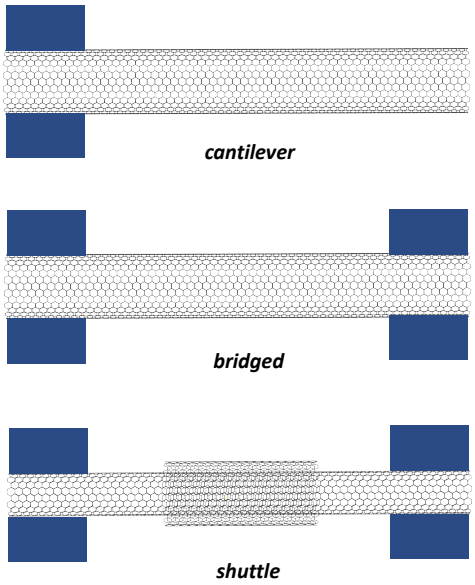

Figure 1: Schematic diagrams of the nanomechanical resonators studied.

Computational simulations can be applied to study the changes in resonant frequency induced in these devices, providing a foundation to design and optimise their performance. There have been a large number of computational studies exploring the properties of these systems employing a range of different methods, and some reviews of this work are available.[3] In general these systems have been predominantly modelled using continuum mechanics or molecular dynamics (MD) simulations. In continuum models the atoms themselves are neglected and the structure is treated as a continuous microstructure, and a range of models have been applied to the study of CNTs.[3,15–17] One example is the study of graphene-resonator composed of a suspended graphene-ribbon. Resonant frequencies in the range 750-1200 GHz depending on the configuration of the device were determined.[18] It has also been shown that there is a decrease in the resonant frequency as the aspect ratio of the nanotube increases.[17]

MD simulations provide an atomistic description of the system with the potential to pro-

vide a more detailed insight into the vibrational behaviour and the interactions underpinning the function of these systems. These simulations require a force field to describe the interatomic interactions, and established force-fields such as the reactive empirical bond order (REBO)[19] and adaptive intermolecular reactive empirical bond order (AIREBO)[20] potentials are commonly used. In these simulations the resonant frequencies can be determined by applying an external force for an initial period of the simulation that is subsequently removed and the CNT left to oscillate freely with atoms at the edge of the CNT fixed to represent different boundary conditions that arise as a consequence of the different nanoresonator configurations.[21–26] Other atomistic approaches include a molecular structural mechanics method that has been applied to study single and multi-walled CNTs.[27,28] Resonant frequencies in the range of 10 GHz – 1.5 THz depending on the nanotube diameter and length were determined, and it was also found that bridged nanotubes have higher fundamental frequencies than cantilevered ones. Furthermore, the fundamental frequencies of double-walled CNTs are about 10% lower than those of single-walled CNTs of the same outer diameter. The vibrational frequencies associated with the relative motion of the tubes in double-walled nanotubes have been determined based upon the interaction potential calculated using density functional theory (DFT).[13,14] For a (9,0)@(18,0) double-walled carbon nanotube with the movable outer wall, a frequency of 130 GHz was predicted, with a lower value of about 45 GHz for a (5,5)@(10,10) nanotube.[14]

An alternative approach to characterise these systems is to perform a full vibrational frequency analysis to determine the normal modes and their associated frequencies. Previous work has shown that widely used potentials such as REBO perform poorly for the prediction of vibrational frequencies of fullerenes and CNTs,[29] but new potentials designed to predict vibrational frequencies of carbon nanostructures have been reported.[30] In this work, a vibrational frequency analysis is performed for the three types of nanomechanical resonator illustrated in Figure 1. Using an empirical atomistic model the vibrational modes of the

different types of nanoresonator and their dependence on the dimensions of the nanotube are characterised. This allows the mass-sensing capabilities of the different nanoresonator configurations to be assessed. It is shown that a cantilever type nanoresonator has a sensitivity of up to approximately 10^{30} Hz/g for the nanotubes studied that is dependent on the mass absorption site, while the response of a shuttle-type resonator is independent of the absorption site.

Methods

The nanoresonator systems are described using the Murrell-Mottram (MM) potential[31] which represents the interaction between atoms through a sum of two-body and three-body contributions. For a system of N atoms, the potential has the following form:

$$E = \sum_{i}^{N} \sum_{j=i+1}^{N} V_{ij}^{(2)} + \sum_{i}^{N} \sum_{j=i+1}^{N} \sum_{k=j+1}^{N} V_{ijk}^{(3)} \tag{1}$$

where

$$V_{ij}^{(2)} = -D(1 + a_2\rho_{ij}) \exp(-a_2\rho_{ij}) \tag{2}$$

$$V_{ijk}^{(3)} = DP(Q_1, Q_2, Q_3) \exp(-a_3 Q_1) \tag{3}$$

$$\rho_{ij} = (r_{ij} - r_e)/r_e. \tag{4}$$

The two-body potential $V_{ij}^{(2)}$ is represented by a Rydberg function, where r_{ij} is the distance between atoms i and j. D and r_e are parameters that are chosen such that the energy and structure are described accurately. The terms $\exp(-a_2\rho_{ij})$ and $\exp(-a_3 Q_1)$ are damping functions which depend on the parameters a_2 and a_3, and they ensure the potential converges to zero energy at infinite interatomic separation. $P(Q_1, Q_2, Q_3)$ is a quartic polynomial

$$
\begin{aligned}
P(Q_1, Q_2, Q_3) &= c_0 + c_1 Q_1 + c_2 Q_1^2 + c_3 (Q_2^2 + Q_3^2) \\
&+ c_4 Q_1^3 + c_5 Q_1 (Q_2^2 + Q_3^2) \\
&+ c_6 (Q_3^3 - 3 Q_3 Q_2^2) + c_7 Q_1^4 + c_8 Q_1^2 (Q_2^2 + Q_3^2) \\
&+ c_9 (Q_2^2 + Q_3^2)^2 + c_{10} Q_1 (Q_3^3 - 3 Q_3 Q_2^2) \qquad (5)
\end{aligned}
$$

where Q_i are symmetrical coordinates

$$
\begin{aligned}
Q_1 &= \frac{1}{\sqrt{3}} (\rho_{ij} + \rho_{ik} + \rho_{jk}) \qquad (6) \\
Q_2 &= \frac{1}{\sqrt{2}} (\rho_{ij} + \rho_{ik}) \qquad (7) \\
Q_3 &= \frac{1}{\sqrt{6}} (2\rho_{ij} - \rho_{ik} - \rho_{jk}). \qquad (8)
\end{aligned}
$$

Table 1: Parameters for the Murrell-Mottram potential with dispersion for carbon.

Parameter	MM^{Vib+D}
D / eV	6.298
r_e / Å	1.313
a_2	7.428
a_3	8.072
c_0	7.788
c_1	3.917
c_2	-17.503
c_3	-51.427
c_4	99.263
c_5	-39.772
c_6	70.505
c_7	73.262
c_8	3.831
c_9	65.696
c_{10}	-85.307
s_6	2.06
C_6 / J nm^6 mol^{-1}	1.75
R_0 / Å	1.75
α	28.00

The term Q_1 describes the perimeter of the interaction triangles, while Q_2 and Q_3 describe

the distortions of the triangles from being equilateral and c_0 to c_{10} are parameters that need to be determined. Parameters for carbon have been reported by Eggen *et al.*,[32] wherein the potential was fitted to the phonon frequencies and elastic constants of diamond and to the cohesive energy and intralayer spacing of graphite in addition to other structural data. However, these parameters based upon diamond do not account for π-bonding electronic effects, and, as a consequence, are not well suited to describe CNTs. To improve the description of CNTs, the MM potential was parameterised to describe the structure and vibrational frequencies of carbon nanomaterials using a Monte-Carlo hessian-matching approach to reproduce data from density functional theory calculations.[30] More specifically, the parameters were optimised to reproduce the hessian matrix and structure of C_{60}, and the resulting potential was applied to study the vibrational spectroscopy of single-walled carbon nanotubes and graphene.

More recently, the potential was extended to model multi-layer carbon materials through the inclusion of Van der Waals interactions between the layers,[33] where the potential has the form

$$E = \sum_{i}^{N} \sum_{j=i+1}^{N} V_{ij}^{(2)} + \sum_{i}^{N} \sum_{j=i+1}^{N} \sum_{k=j+1}^{N} V_{ijk}^{(3)} + \sum_{i}^{N} \sum_{j=i+1}^{N} V_{ij}^{(Disp)} \tag{9}$$

where

$$V_{ij}^{(Disp)} = -s_6 \sum_{i}^{N-1} \sum_{j=i+1}^{N} \frac{C_6}{R_{ij}^6} f_{dmp}(R_{ij}) \tag{10}$$

and C_6 is the dispersion coefficient for a pair of carbon atoms, s_6 is a global scaling factor to account for the different behaviour of the intermolecular potential especially at intermediate distances, and R_{ij} is the inter-atomic distance between atoms ij. The damping function $f_{dmp}(R_{ij})$ is given by

$$f_{dmp}(R_{ij}) = \frac{1}{1 + e^{-\alpha(\frac{R_{ij}}{R_0} - 1)}} \tag{11}$$

where R_0 is the sum of atomic Van der Waals radii and α is a damping parameter. This function removes the singularity at $R_{ij} = 0$ and ensures that the dispersion contribution

becomes insignificant below the Van der Waals separation and, consequently, the covalent bonds described by the MM potential are not significantly affected. The dispersion term has been optimized such that it predicts the interlayer spacing and the frequency of the shear mode of bilayer graphene correctly, and the full parameters for the potential are given in Table 1. For the calculations presented here, single-walled nanotubes were described using the potential without the dispersion contribution (equation 1) and for the double-walled nanotubes the dispersion term was included (equation 9).

Table 2: Dimensions of the nanotubes studied.

Nanotube	Diameter (nm)	Length (nm)	Aspect Ratio (L/D)	Number of Atoms
(5,5)-A	0.68	4.80	7.1	400
(5,5)-B	0.68	14.6	21.5	1200
(5,5)-C	0.68	24.5	36.0	2000
(10,10)-A	1.36	4.80	3.5	800
(10,10)-B	1.36	14.6	10.8	2400
(10,10)-C	1.36	24.5	18.0	4000
(15,15)-A	2.03	4.80	2.4	1200
(15,15)-B	2.03	14.6	7.2	3600
(15,15)-C	2.03	24.5	12.1	6000

Structures were optimized using the conjugate gradient method with a gradient convergence criterion of 10^{-8} E_h Å^{-1}, and a spherical cut-off was applied to the potential with a radius of 8 Å. Harmonic vibrational frequencies and normal modes were calculated through diagonalisation of the mass-weighted hessian matrix, where the required second derivatives are evaluated analytically. The effects of the clamping of the nanotubes on the vibrational frequencies has been modelled by applying a very large mass (1×10^7 a.m.u) to the appropriate carbon atoms in the mass-weighting of the hessian matrix. This has the effect of keeping these atoms fixed in the vibrational analysis, and the vibrational modes associated with the fixed atoms have a frequency that is approximately zero. For the cantilever resonator, the first six rings of carbon atoms at one end of the nanotube were fixed through the mass-weighting, which constitutes 120 atoms for a (10,10) CNT. For the bridged resonator, six

rings of carbon atoms were fixed at each end of the CNT, and for the shuttle resonator all of the carbon atoms of the inner tube were fixed. The vibrational frequencies have been studied for armchair CNTs of different dimensions, and the dimensions and notation for these tubes are given in Table 2. Owing to the computational cost, the longest nanotubes studied here are ≈25 nm in length, which is shorter than those used typically used in experimental investigations. However, studies on smaller nanotubes do enable a direct comparison between the properties of the different resonator configurations and allow for the convergence of the frequencies with respect to the dimensions of the nanotubes to be studied. The notation used to describe the nanotubes follows the standard chiral indices (n,m) notation,[34] and the letters A, B and C denote the length of the nanotubes. (5,5)@(10,10)-B is an example of a double-walled nanotube, and comprises the (5,5)-B nanotube in the (10,10)-B nanotube and would have a length of 14.6 nm. While only armchair nanotubes, where the indices n and m are equal, are considered here, previous studies have found similar behaviour between armchair and zigzag nanotubes for these systems.[27] The response of the resonators to an adsorbed mass was simulated by varying the mass of a six membered carbon ring, this was done for different positions on the resonators to explore their sensitivity with respect to the location of the absorption site.

Results and Discussion

Cantilever resonator

The vibrational analysis performed here provides a complete picture of the vibrational modes of the resonator systems. The number of vibrational modes of these systems is extremely large and Figure 2 illustrates just six key characteristic low frequency vibrational modes of the cantilever style nanoresonator. There are many more vibrational modes of higher frequency, however, these can generally be characterised as higher order vibrational modes

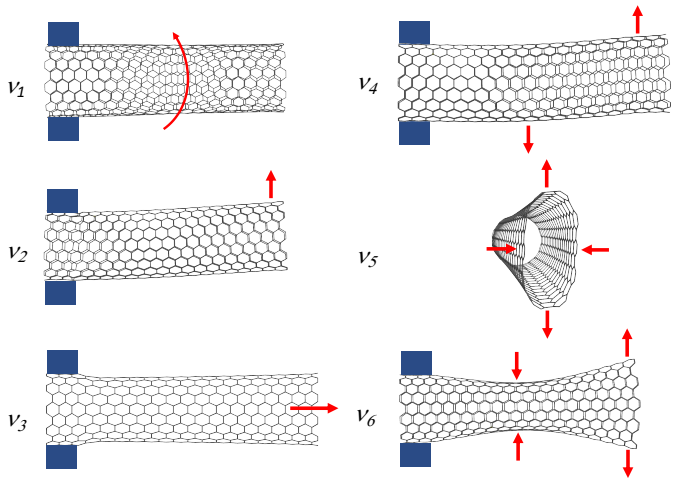

Figure 2: Illustration of the key vibrational modes for the cantilever resonator. The amplitudes of the vibrations have been amplified to allow for the motion to be distinguished more clearly. The long axis of the nanotube lies in the z direction

(i.e. with additional nodes) of the vibrational modes shown. For the nanotubes with larger diameter there are also many vibrational modes that correspond to complex deformations of the tube that are difficult to characterise.

The first vibrational mode ν_1 is singly degenerate and corresponds to a rotation of the tube around its axis. The second mode corresponds to the flexural vibrational of the whole tube and is the mode that is typically studied for this type of resonator. This mode is doubly degenerate owing to the motion can occur in x and y directions (where the nanotube lies on the z-axis). ν_3 is an elongation of the tube along its axis, and is singly degenerate. ν_4 is related to ν_3, however, as the end of the tube moves in one direction the remainder of the tube moves in the opposite direction to give a snake-like motion. ν_5 is a distortion at the free and open end of the nanotube, while ν_6 corresponds to a radial opening of the end of the tube in conjunction with a compression at the centre of the tube. These latter two modes clearly arise owing to the choice of an open-ended nanotube rather than a capped end.[35]

The computed frequencies of these modes for a set of nanotubes with varying lengths and

Table 3: Calculated vibrational frequencies (in GHz) for the cantilever nanoresonator.

Nanotube	ν_1	ν_2	ν_3	ν_4	ν_5	ν_6
(5,5)-A	585	132	1073	666	1625	1748
(5,5)-B	177	75	324	204	1622	1700
(5,5)-C	105	75	189	144	1625	1700
(10,10)-A	585	231	1070	878	405	627
(10,10)-B	177	138	324	345	393	405
(10,10)-C	105	138	192	252	396	399
(15,15)-A	585	291	1055	962	216	582
(15,15)-B	177	186	324	432	174	264
(15,15)-C	105	186	192	327	174	192
(5,5)@(10,10)-A	589	205	1091	829	-	-
(5,5)@(10,10)-B	174	119	329	310	-	-
(10,10)@(15,15)-A	588	270	1077	940	-	-

*The nanotubes have lengths: A - 4.8 nm, B - 14.6 nm and C - 24.5 nm and diameters: (5,5) - 0.68 nm, (10,10) - 1.36 nm and (15,15) - 2.03 nm.

diameter are shown in Table 3. The different vibrational modes show a varying behaviour in their dependence on the structure of the nanotube. The frequency of ν_1 is independent of the tube diameter but reduces as the length of the tube increases. For the longest tube studied here, a frequency of 105 GHz is predicted. There is also only a small change in frequency for the double-walled carbon nanotubes compared with their singled-walled analogues. ν_3 shows a similar behaviour to ν_1 in that the frequency is dependent on the length of the tube and not the diameter, with the exception of the shortest nanotubes studied. ν_4 shows an increase in frequency as the diameter increases, while decreasing with increasing tube length. With the exception of the shortest nanotubes, the frequencies for ν_5 and ν_6 show little dependence on the length of the tube but decrease with increasing diameter.

We focus our discussion on ν_2 since this is the most important vibrational mode in the context of mass-sensing nanoresonators. This mode has been studied previously in the literature allowing the trends observed here to be compared with the findings from different computational approaches. The calculations show a clear increase in the frequency of this mode as the diameter of the nanotube increases which is consistent with previous work.[24] The frequency also decreases with increasing length. A similar dependence on the length of

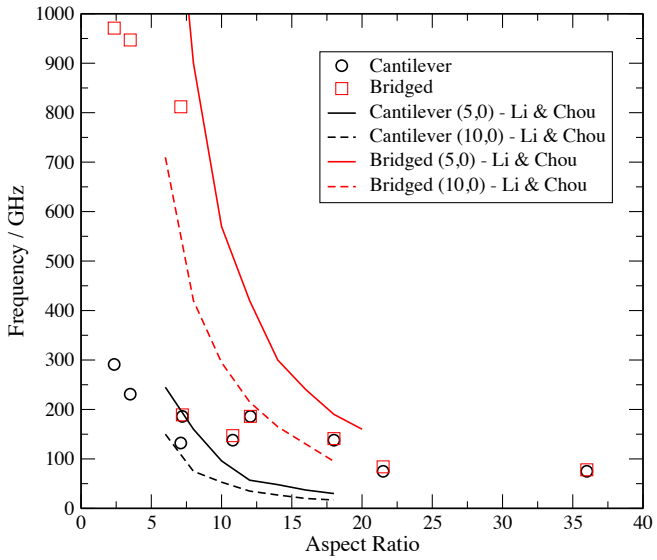

Figure 3: Variation of the frequency for the flexural modes with aspect ratio of the nanotube for the cantilever and bridged resonators.

tube has also been observed in previous computational studies. In this study, nanotubes of sufficient length have been studied to see convergence of the frequency with respect to the length of the tube. Using a MD approach with the REBO potential, Arash et al.[24] reported a decrease in the resonant frequency as the length of the nanotube increases. Convergence of the frequency with respect to the length of the tube was not observed but the length of tubes studied, up to about 9.5 nm, is considerably shorter that the longest tubes considered here. The MD approach predicted a frequency of 182 GHz for a 9.5 nm (5,5) nanotube, which compares with a value of 82 GHz for a 9.5 nm (5,5) nanotube using the approach used in this work. The dependence of the resonant frequency on the dimensions is captured by examining its variation with the aspect ratio of the tube. This follows previous studies[17,27] and provides a convenient approach to compare results for nanotubes of different lengths and diameters, although it will neglect more subtle dependencies on the length and diameter. This dependence is shown in Figure 3 which also shows results adapted from the work of Li and Chou.[27] Focusing on the data for the cantilever configuration, there is close agreement between the results for nanotubes with a smaller aspect ratio. For the larger aspect ratio nanotubes, higher frequencies are predicted in this work and the reason for this difference

could be associated with the force field or the approach used to determine the frequencies.

Results are also shown for double-walled nanotubes, where the calculations find the frequency for ν_2 to lie between the frequencies of the component single-walled nanotubes. For example a value of 119 GHz for (5,5)@(10,10)-B is found which compares with values of 75 GHz for (5,5)-B and 138 GHz for (10,10)-B. This represents the balance between the increasing stiffness for the double-walled tubes[36] and their increased mass. This is consistent with the results of previous studies. Using a MD approach for a cantilever styled resonator,[22] the frequency for a double-walled nanotube was found to be less than for the outer single-walled tube. Also a continuum approach based study for a bridged resonator showed the frequency for the double-walled nanotube to lie in between those for the inner and outer tubes,[15] and the fundamental frequencies of double-walled carbon nanotubes have been found to be 10% lower than those of single-walled carbon nanotubes of the same outer diameter.[28] Frequencies are not reported for modes ν_5 and ν_6, which involve distortion of the open end of the nanotube, since the corresponding modes cannot be reliably identified for the double-walled nanotubes. For the double-walled nanotubes there is an additional type of mode that corresponds to the rotation of the tubes along their axes relative to each other. These frequencies are calculated to be 678 GHz, 384 GHz and 604 GHz for the (5,5)@(10,10)-A, (5,5)@(10,10)-B and (10,10)@(15,15)-A nanotubes, respectively.

Bridged resonator

Next we consider the bridged resonator configuration, and the key vibrational modes are shown in Figure 4. There is a direct correspondence between these modes and the vibrational modes for the cantilever resonator, with the exception that the modes involving the distortion of the open end of the tube are no longer present. The dependence of the calculated frequencies are given in Table 4. ν_1 corresponds to the vibrational mode that is

Table 4: Calculated vibrational frequencies (in GHz) for the bridged nanoresonator.

Nanotube	ν_1	ν_2	ν_3	ν_4	ν_5
(5,5)-A	812	1400	1733	2533	1775
(5,5)-B	84	372	222	678	1700
(5,5)-C	78	213	150	393	1697
(10,10)-A	947	1400	1913	2407	684
(10,10)-B	147	369	351	681	405
(10,10)-C	141	213	255	393	399
(15,15)-A	971	1397	1874	2159	627
(15,15)-B	189	369	417	678	192
(15,15)-C	186	213	323	393	177
(5,5)@(10,10)-B	129	372	318	910	692

*The nanotubes have lengths: A - 4.8 nm, B - 14.6 nm and C - 24.5 nm and diameters: (5,5) - 0.68 nm, (10,10) - 1.36 nm and (15,15) - 2.03 nm.

relevant for the mass sensing applications and we focus our discussion on this mode. Similar to the cantilever configuration, the frequencies of this mode increase with the diameter of the tube. Also while the frequency decreases with the length of the tube, it has nearly converged for the longest tubes studied. Interestingly, the value of the frequency is close to the corresponding value for the cantilever resonator. For example, the frequency of 186 GHz is obtained for the (15,15)-C nanotube both in cantilever and bridged configurations. Previous studies that considered shorter nanotubes have concluded that the frequencies for the bridged resonator are higher, but the results presented here suggest that the frequencies for the two resonators approach the same value with increasing length of the tube. The dependence on the frequency of this mode with respect to the aspect ratio is also shown in Figure 3. For short aspect ratios the frequencies are much higher than those of the cantilever resonator, but the convergence for larger aspect ratios is evident. The results of this work are also in close agreement with the molecular structural mechanics model of Li and Chou,[27] and also calculations using the Euler-Bernoulli beam model which showed a decrease in frequency as the aspect ratio of the tubes increases.[17] The ν_2 and ν_4 modes do not involve motion perpendicular to the axis of the tube, and the frequencies show little dependence on tube diameter but decrease with increasing length of the tube. For both the ν_3 and ν_5 modes the frequency decreases as the length increases but show different trends with respect

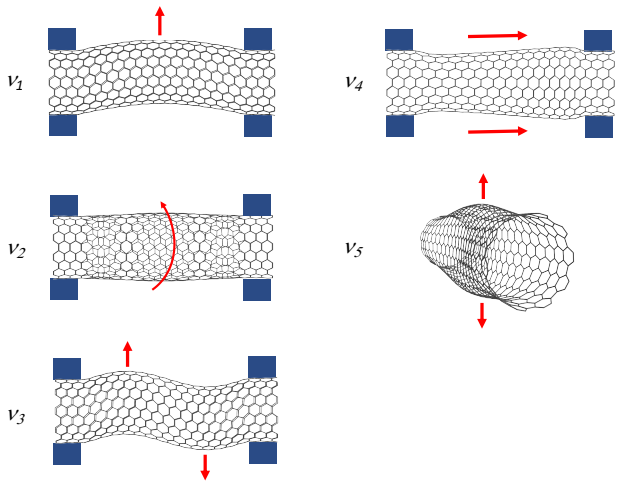

Figure 4: Illustration of the key vibrational modes for the bridged resonator. The amplitudes of the vibrations have been amplified to allow for the motion to be distinguished more clearly. The long axis of the nanotube lies in the z direction

to diameter. Frequencies have also been computed for the (5,5)@(10,10)-B double-walled nanotube. We focus on this nanotube since it provides a closer representation of experiments than the shorter nanotubes. Similar to the behaviour for the double-walled nanotube cantilever resonator, the calculated frequency of the flexural mode (ν_1) lies in between the values calculated for the individual single-walled nanotubes.

Table 5: Calculated vibrational frequencies (in GHz) for the shuttle nanoresonator.

Nanotube	ν_1	ν_2	ν_3	ν_4	ν_5
(5,5)@(10,10)-A	116	328	1019	1584	1685
(5,5)@(10,10)-B	68	375	1014	1245	1575
(10,10)@(15,15)-A	121	277	361	1595	1709

*The nanotubes have lengths: A - 4.8 nm, B - 14.6 nm and C - 24.5 nm and diameters: (5,5) - 0.68 nm, (10,10) - 1.36 nm and (15,15) - 2.03 nm.

Shuttle resonator

The shuttle resonator represents a significantly different approach where the relevant vibrational modes correspond to the relative motion of the nanotubes. While this type of resonator has not been realised in practice, resonator devices that depend on the relative motion of

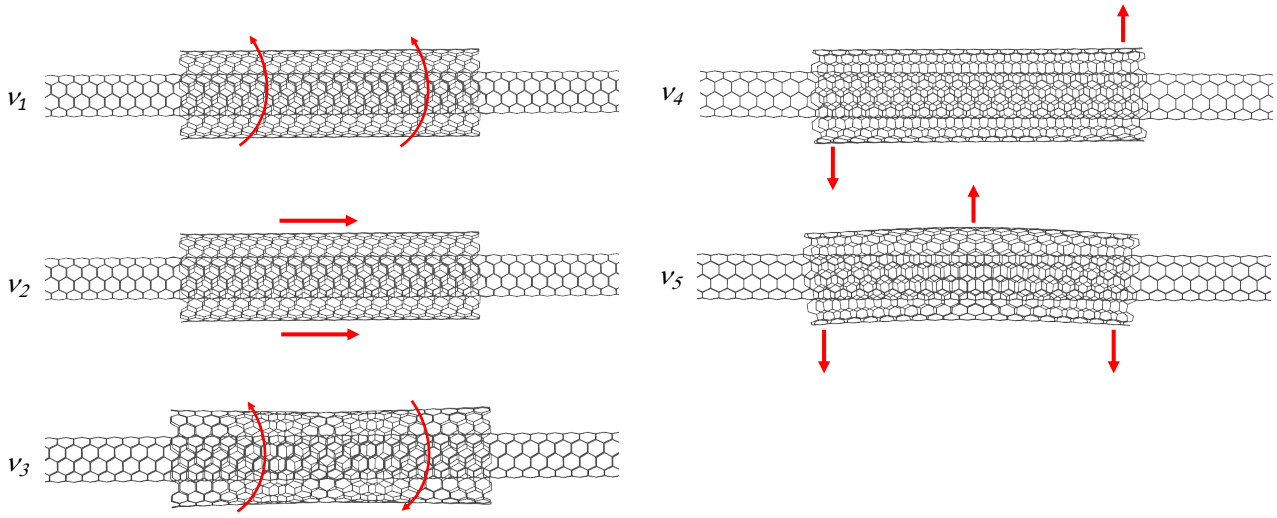

Figure 5: Illustration of the key vibrational modes for the shuttle resonator. The amplitudes of the vibrations have been amplified to allow for the motion to be distinguished more clearly. The long axis of the nanotube lies in the z direction

multi-walled nanotubes have been developed.[1] These fundamental vibrational modes for the shuttle resonator are shown in Figure 5, and correspond to the rotation, linear motion, tilting and bending of the outer tube. The calculated vibrational frequencies for three resonator systems capturing a variation in length and diameter of the shuttle are given in Table 5. The frequencies for the bending (ν_5) and tilting (ν_4) vibrational modes are considerably higher than for the flexural modes of the cantilever and bridged resonators. The two modes with lowest frequency correspond to the relative rotation (ν_1) and the relative linear motion (ν_2) of the tubes. The ν_1 mode has been studied previously and discussed in the context of a mass-sensing device.[13,14] The calculations predict a frequency of 116 GHz for (5,5)@(10,10)-A which decreases to 68 GHz as the length of the shuttle increases. There is little change in frequency for the wider diameter tubes, which represents an increase in inter-wall separation of 3.4 Å to 4.2 Å. The calculated frequency of this mode is consistent with previous work where it was determined based upon a potential computed using DFT[14] giving a value of 46 GHz, which is in good agreement with the value reported here.

Mass sensing

The calculations provide an opportunity to explore the response of the resonators to the adsorption of a mass. This is modelled by assuming that the mass is adsorbed on a single six membered ring and the mass is evenly distributed between the six carbon atoms. The response of the resonator is then determined by modifying the mass of these carbon atoms for the mass-weighting of the hessian. The calculations have used the (10,10)-B nanotube for the cantilever and bridged resonators and (5,5)@(10,10)-A for the shuttle resonator, and for the cantilever resonator the ν_2 mode (Figure 2) is studied, ν_1 (Figure 4) for the bridged resonator and ν_1 (Figure 5) for the shuttle resonator. The response of the resonators with respect to the position of the adsorbed mass is also studied and Figure 6 shows the various locations of the adsorbed mass that have been considered along with the change in the calculated frequency as the applied mass is increased.

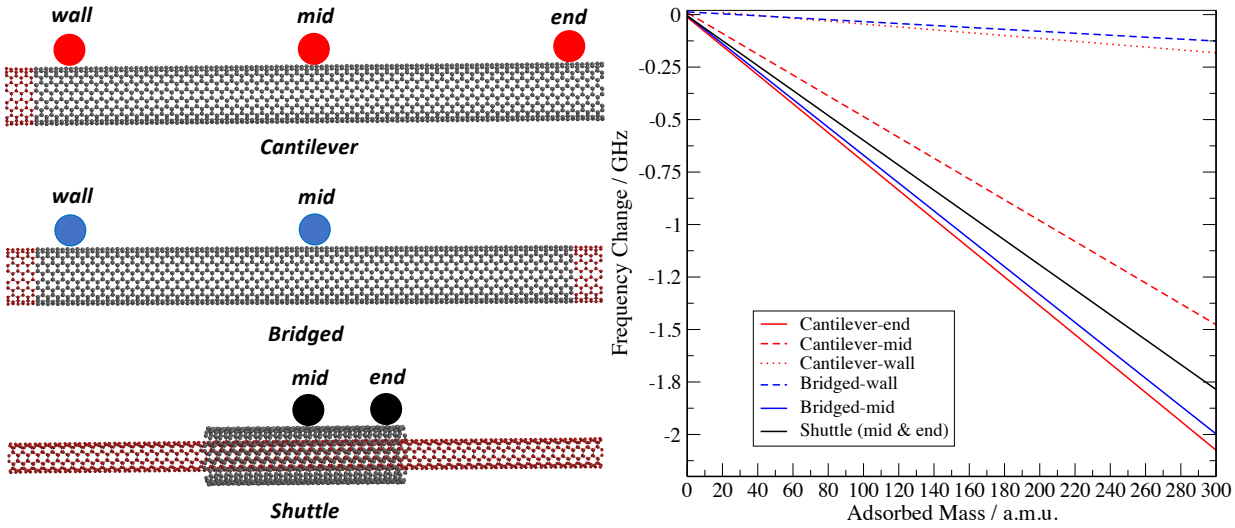

Figure 6: Change in frequency on the addition of a mass for the different resonators. Red atoms denote atoms that are frozen in the vibrational analysis (100 a.m.u $\approx$ 0.17 zg)

.

For all of the resonators studied here, there is a linear decrease in the frequency as the mass increases. One factor to consider is that in this study harmonic vibrational frequen-

cies are computed and additional effects may be observed if anharmonicity was considered. In previous studies examining the response of the cantilever and bridged resonators to an applied mass also showed a decrease in frequency as the applied mass increases.[17,37] For the cantilever resonator, three positions of for the adsorbed mass are considered, and the change in the resonant frequency is sensitive to the location of the adsorbed mass. There is no significant response for the mass adsorbed near the wall, while there is a shift of about 2 GHz for a mass of 300 a.m.u ($\approx$ 0.5 zg). This variation will contribute to the distribution of frequency shifts observed in experiment.[7] The response of the bridged resonator shows a similar behaviour, with the predicted frequency shift for the mass at the centre of the nanotube being close to the value for the end of the cantilever resonator. The gradient of the lines is an important factor in the sensitivity of a mass-sensing device. The gradient for the end position of the cantilever resonator is of the order to 10^{30} Hz/g, which is in reasonable agreement with previous work,[37] and will depend on the dimensions of the nanotube. Finally we consider the shuttle resonator which shows a response that is only slightly smaller than the largest response of the cantilever and bridged resonators, but crucially shows no dependence on the position of the mass.

Conclusions

The vibrational modes for three different types of mass-sensing nanomechanical resonators have been characterised through a harmonic vibrational frequency analysis using a potential designed to describe the vibrational frequencies of carbon systems. The different resonator configurations are represented by applying a large mass to the appropriate carbon atoms in the mass-weighting of the hessian matrix. The resonant frequencies of these devices have been studied as the length and diameter of the nanotube is varied. For the flexural modes which are relevant for mass-sensing resonator devices, the calculations show the resonant fre-

quency to increase as the tube diameter increases. The frequency is also shown to decrease with increasing length of the tube, although for the longest tubes considered, the frequency is found to have converged with respect to the length. For these longest nanotubes, the frequencies for cantilever and bridged resonators are very similar. For double-walled nanotubes the resonant frequencies lie between the frequencies of the component single-walled nanotubes which represents the balance between the increasing stiffness for the double-walled tubes and their increased mass. The vibrational modes for a shuttle resonator have also been determined, and the lowest frequency mode was found to correspond to the relative rotation of the nanotubes with frequencies in the range 70 – 120 GHz.

Calculations exploring the sensitivity of the resonators to the adsorption of an applied mass show predict a sensitivity of up to 10^{30} Hz/g although the response of the flexural modes of suspended nanotubes is dependent on the location of the adsorbed mass and this will contribute to the distribution of frequency shifts that are observed in a device. The response in the frequency for the shuttle resonator based upon the relative rotational motion in double-walled nanotubes is shown to be independent of the position of the adsorbed mass, which represents a favourable attribute for a mass-sensing device.

Conflicts of Interest

There are no conflicts of interest to declare.

References

(1) Jensen, K.; Girit, C.; Mickelson, W.; Zettl, A. Tunable Nanoresonators Constructed from Telescoping Nanotubes. *Phys. Rev. Lett.* **2006**, *96*, 215503.

(2) Eom, K.; Park, H. S.; Yoon, D. S.; Kwon, T. Nanomechanical resonators and their

applications in biological/chemical detection: Nanomechanics principles. *Phys. Rep.* **2011**, *503*, 115 – 163.

(3) Arash, B.; Jiang, J.-W.; Rabczuk, T. A review on nanomechanical resonators and their applications in sensors and molecular transportation. *Appl. Phys. Rev.* **2015**, *2*, 021301.

(4) Zhao, C.; Montaseri, M. H.; Wood, G. S.; Pu, S. H.; Seshia, A. A.; Kraft, M. A review on coupled MEMS resonators for sensing applications utilizing mode localization. *Sensor. Actuat. A* **2016**, *249*, 93 – 111.

(5) Wang, X.; Zhu, D.; Yang, X.; Yuan, L.; Li, H.; Wang, J.; Chen, M.; Deng, G.; Liang, W.; Li, Q.; Fan, S.; Guo, G.; Jiang, K. Stressed carbon nanotube devices for high tunability, high quality factor, single mode GHz resonators. *Nano Res.* **2018**, *11*, 5812–5822.

(6) Peng, H. B.; Chang, C. W.; Aloni, S.; Yuzvinsky, T. D.; Zettl, A. Ultrahigh Frequency Nanotube Resonators. *Phys. Rev. Lett.* **2006**, *97*, 087203.

(7) Jensen, K.; Kim, K.; Zettl, A. An atomic-resolution nanomechanical mass sensor. *Nat. Nanotechnol.* **2008**, *3*, 533–537.

(8) Lassagne, B.; Garcia-Sanchez, D.; Aguasca, A.; Bachtold, A. Ultrasensitive Mass Sensing with a Nanotube Electromechanical Resonator. *Nano Lett.* **2008**, *8*, 3735–3738.

(9) Poncharal, P.; Wang, Z. L.; Ugarte, D.; de Heer, W. A. Electrostatic Deflections and Electromechanical Resonances of Carbon Nanotubes. *Science* **1999**, *283*, 1513–1516.

(10) Hüttel, A. K.; Steele, G. A.; Witkamp, B.; Poot, M.; Kouwenhoven, L. P.; van der Zant, H. S. J. Carbon Nanotubes as Ultrahigh Quality Factor Mechanical Resonators. *Nano Lett.* **2009**, *9*, 2547–2552.

(11) Eichler, A.; Moser, J.; Chaste, J.; Zdrojek, M.; Wilson-Rae, I.; Bachtold, A. Nonlinear damping in mechanical resonators made from carbon nanotubes and graphene. *Nat. Nanotechnol.* **2011**, *6*, 339–342.

(12) Chaste, J.; Eichler, A.; Moser, J.; Ceballos, G.; Rurali, R.; Bachtold, A. A nanomechanical mass sensor with yoctogram resolution. *Nat. Nanotechnol.* **2012**, *7*, 301–304.

(13) Bichoutskaia, E.; Popov, A. M.; Lozovik, Y. E.; Ershova, O. V.; Lebedeva, I. V.; Knizhnik, A. A. Modeling of an ultrahigh-frequency resonator based on the relative vibrations of carbon nanotubes. *Phys. Rev. B* **2009**, *80*, 165427.

(14) Bichoutskaia, E.; Popov, A. M.; Lozovik, Y. E.; Ershova, O. V.; Lebedeva, I. V.; Knizhnik, A. A. Nanoresonator Based on Relative Vibrations of the Walls of Carbon Nanotubes. *Fuller. Nanotub. Carbon Nanostructures* **2010**, *18*, 523–530.

(15) Natsuki, T.; Ni, Q.-Q.; Endo, M. Analysis of the vibration characteristics of double-walled carbon nanotubes. *Carbon* **2008**, *46*, 1570 – 1573.

(16) Georgantzinos, S.; Anifantis, N. Carbon nanotube-based resonant nanomechanical sensors: A computational investigation of their behavior. *Physica E* **2010**, *42*, 1795 – 1801.

(17) Natsuki, T.; Matsuyama, N.; Shi, J.-X.; Ni, Q.-Q. Vibration analysis of nanomechanical mass sensor using carbon nanotubes under axial tensile loads. *Appl. Phys. A* **2014**, *116*, 1001–1007.

(18) Kitipornchai, S.; He, X. Q.; Liew, K. M. Continuum model for the vibration of multilayered graphene sheets. *Phys. Rev. B* **2005**, *72*, 075443.

(19) Brenner, D. W.; Shenderova, O. A.; Harrison, J. A.; Stuart, S. J.; Ni, B.; Sinnott, S. B. A second-generation reactive empirical bond order (REBO) potential energy expression for hydrocarbons. *J. Phys. Condens. Matter* **2002**, *14*, 783–802.

(20) Stuart, S. J.; Tutein, A. B.; Harrison, J. A. A reactive potential for hydrocarbons with intermolecular interactions. *J. Chem. Phys.* **2000**, *112*, 6472–6486.

(21) Duan, W. H.; Wang, C. M.; Zhang, Y. Y. Calibration of nonlocal scaling effect parameter for free vibration of carbon nanotubes by molecular dynamics. *J. Appl. Phys.* **2007**, *101*, 024305.

(22) Kang, J. W.; Choi, Y. G.; Kim, Y.; Jiang, Q.; Kwon, O. K.; Hwang, H. J. The frequency of cantilevered double-wall carbon nanotube resonators as a function of outer wall length. *J. Phys. Condens. Matter* **2009**, *21*, 385301.

(23) Feng, E. H.; Jones, R. E. Equilibrium thermal vibrations of carbon nanotubes. *Phys. Rev. B* **2010**, *81*, 125436.

(24) Arash, B.; Wang, Q.; Varadan, V. K. Carbon Nanotube-Based Sensors for Detection of Gas Atoms. *J. Nanotechnol. Eng. Med.* **2011**, *2*, 021010.

(25) Pine, P.; Yaish, Y. E.; Adler, J. The effect of boundary conditions on the vibrations of armchair, zigzag, and chiral single-walled carbon nanotubes. *J. Appl. Phys.* **2011**, *110*, 124311.

(26) Arash, B.; Wang, Q. Detection of gas atoms with carbon nanotubes. *Sci. Rep.* **2013**, *3*, 1782.

(27) Li, C.; Chou, T.-W. Single-walled carbon nanotubes as ultrahigh frequency nanomechanical resonators. *Phys. Rev. B* **2003**, *68*, 073405.

(28) Li, C.; Chou, T.-W. Vibrational behaviors of multiwalled-carbon-nanotube-based nanomechanical resonators. *Appl. Phys. Lett.* **2004**, *84*, 121–123.

(29) Do, H.; Besley, N. A. Calculation of the vibrational frequencies of carbon clusters and fullerenes with empirical potentials. *Phys. Chem. Chem. Phys.* **2015**, *17*, 3898–3908.

(30) Tailor, P. M.; Wheatley, R. J.; Besley, N. A. An empirical force field for the simulation of the vibrational spectroscopy of carbon nanomaterials. *Carbon* **2017**, *113*, 299 – 308.

(31) Murrell, J. N.; Mottram, R. E. Potential energy functions for atomic solids. *Mol. Phys.* **1990**, *69*, 571–585.

(32) Eggen, B. R.; Johnston, R. L.; Murrell, J. N. Carbon cluster structures and stabilities predicted from solid-state potentials. *J. Chem. Soc., Faraday Trans.* **1994**, *90*, 3029.

(33) Tailor, P. M.; Wheatley, R. J.; Besley, N. A. Simulation of the Raman spectroscopy of multi-layered carbon nanomaterials. *Phys. Chem. Chem. Phys.* **2018**, *20*, 28001–28010.

(34) Qin, L.-C. Determination of the chiral indices (n,m) of carbon nanotubes by electron diffraction. *Phys. Chem. Chem. Phys.* **2007**, *9*, 31–48.

(35) Besley, N. A.; Titman, J. J.; Wright, M. D. Theoretical Study of the 13C NMR Spectroscopy of Single-Walled Carbon Nanotubes. *J. Am. Chem. Soc.* **2005**, *127*, 17948–17953.

(36) Ru, C. Q. Effective bending stiffness of carbon nanotubes. *Phys. Rev. B* **2000**, *62*, 9973–9976.

(37) Li, C.; Chou, T.-W. Mass detection using carbon nanotube-based nanomechanical resonators. *Appl. Phys. Lett.* **2004**, *84*, 5246–5248.

TOC Graphic